*J. Fluid Mech.* (2007), *vol.* 591, *pp.* 481–494.  
doi:10.1017/S0022112007008452 Printed in the United Kingdom

# Nonlinear three-dimensional interfacial flows with a free surface

E. I. PĂRĂU, J.-M. VANDEN-BROECK AND M. J. COOKER

School of Mathematics, University of East Anglia, Norwich, NR4 7TJ, UK

(Received 13 December 2006 and in revised form 23 July 2007)

A configuration consisting of two superposed fluids bounded above by a free surface is considered. Steady three-dimensional potential solutions generated by a moving pressure distribution are computed. The pressure can be applied either on the interface or on the free surface. Solutions of the fully nonlinear equations are calculated by boundary-integral equation methods. The results generalize previous linear and weakly nonlinear results. Fully localized gravity–capillary interfacial solitary waves are also computed, when the free surface is replaced by a rigid lid.

## 1. Introduction

We consider a three-dimensional steady potential flow in which a given distribution of pressure moves at constant velocity $U$ on the interface between two fluids, with a lighter fluid of density $\rho_2$ lying above a heavier one of density $\rho_1$. The lower fluid is of infinite depth and the upper fluid layer is bounded above by a free surface. This models, in an inverse way, interfacial flows past submerged bodies on the interface. We also consider problems where the given pressure is applied on the free surface.

In the last half-century there have been a number of investigations of forced waves which propagate at the interface of two fluids (see e.g. Hudimac 1961; Crapper 1967; Keller & Munk 1970; Yih & Zhu 1989; Tulin & Miloh 1991; Avital & Miloh 1998). Some authors have considered the effect of a free surface on the two-layer flow, such as Yeung & Nguyen (1999) and Wey, Lu & Dai (2005).

It was shown that the wave system at the interface or at the free surface is determined by a surface-wave mode and an internal-wave mode. There are also experimental observations of the so-called 'dead-water' effect (first reported by Ekman 1904) and of narrow V-wakes in SAR images (see Hudimac 1961).

Most of these previous studies are either linear or weakly nonlinear. In this paper we complement them by presenting fully nonlinear solutions. The numerical procedure combines ideas developed by Forbes (1989), Părău & Vanden-Broeck (2002), Părău, Vanden-Broeck & Cooker (2005*a*, *b*, 2007). This study involves integro-differential equation formulations obtained by using Green's second identity and the dynamic boundary conditions.

Three-dimensional solitary interfacial waves are also computed when the upper layer is bounded by a rigid lid. Both gravity and interfacial tension are included in the dynamic boundary condition and the given pressure distribution is eliminated. These waves have damped oscillations in the direction of propagation, as reported in the two-dimensional case (Dias & Iooss 1996; Laget & Dias 1997; Calvo & Akylas 2003). The waves are also damped in the transverse direction. When the density ratio $R = \rho_2/\rho_1$ is zero, the three-dimensional solitary interfacial waves reduce to

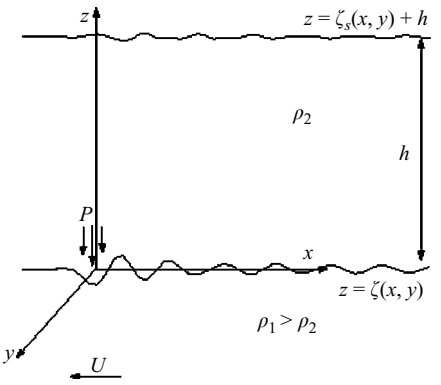


FIGURE 1. Sketch of the problem.

free-surface solitary water waves which were studied by Părău *et al.* (2005*a*, *b*). Our results are also consistent with those of Kim & Akylas (2006) who studied three-dimensional solitary waves for a two-dimensional Benjamin equation. They derived this equation by extending the one-dimensional Benjamin equation which models interfacial waves when the upper layer is bounded by a rigid lid, the interfacial tension is large and the two densities are nearly equal (see Benjamin 1992), and allowing for weak transverse variations.

We present in § 2 computations of gravity flows generated by moving pressure distributions on the interface and on the free surface. The problem is formulated in § 2.1, the numerical method is briefly described in § 2.2 and the numerical results are presented in § 2.3. The three-dimensional capillary–gravity interfacial fully localized solitary waves are discussed in § 3 and some conclusions are presented in § 4.

## 2. Two-layer gravity waves

### 2.1. *Formulation*

The fluids are assumed to be inviscid and incompressible and the flow to be irrotational in both layers. There is no shear between the layers and the free surface, and interfacial tensions are neglected. The subscript 1 refers to the lower fluid, and the subscript 2 to the upper layer. The lower layer is of infinite depth and the upper fluid, which is bounded above by a free surface, has a rest equilibrium thickness $h$. We choose a frame of reference moving with the disturbance (figure 1). We restrict our attention to steady flows. We introduce Cartesian coordinates $x$, $y$, $z$ with the $z$-axis directed vertically upwards. We choose the level $z = 0$ on the undisturbed level of the interface and the $x$-axis in the opposite direction of the velocity $U$. We denote by $z = \zeta(x, y)$ the position of the interface and by $z = \zeta_s(x, y) + h$ the equation of the free surface.

The governing equations in each layer are the Laplace equations

$$\Delta \Phi_i = 0 \quad (i = 1, 2), \tag{2.1}$$

where $\Phi_i$ is the velocity potential in layer $i$. On the interface $z = \zeta(x, y)$, the kinematic and dynamic conditions give

$$\Phi_{ix}\zeta_x + \Phi_{iy}\zeta_y = \Phi_{iz} \quad (i = 1, 2), \tag{2.2}$$

$$\tfrac{1}{2}\rho_1\left(\Phi_{1x}^2 + \Phi_{1y}^2 + \Phi_{1z}^2\right) - \tfrac{1}{2}\rho_2\left(\Phi_{2x}^2 + \Phi_{2y}^2 + \Phi_{2z}^2\right) + (\rho_1 - \rho_2)g\zeta + p_I = \tfrac{1}{2}(\rho_1 - \rho_2)U^2. \tag{2.3}$$

Here, $\rho_i$ are the constant densities and $g$ is the acceleration due to gravity. The pressure distribution which models the disturbance at the interface is $p = p_I$ (specified below as a function of position). Strictly speaking, $p_I$ is the imposed deviation from the hydrostatic pressure term $\rho_2 gh$.

On the free surface $z = \zeta_s(x, y) + h$, we have again the kinematic and dynamic conditions

$$\Phi_{2x}\zeta_{s_x} + \Phi_{2y}\zeta_{s_y} = \Phi_{2z}, \tag{2.4}$$

$$\tfrac{1}{2}\left(\Phi_{2x}^2 + \Phi_{2y}^2 + \Phi_{2z}^2\right) + g(\zeta_s + h) + p_F = \tfrac{1}{2}U^2 + gh, \tag{2.5}$$

where $p_F$ is the pressure distribution which models the disturbance on the free surface. The velocity and radiation boundary conditions at infinity are

$$(\Phi_{1x}, \Phi_{1y}, \Phi_{1z}) \to (U, 0, 0) \quad \text{as } z \to -\infty, \tag{2.6}$$

$$\text{no waves} \quad \text{as } x \to -\infty. \tag{2.7}$$

We shall present in § 2.3, results for $p_I \neq 0$, $p_F = 0$ (pressure applied on the interface) and for $p_I = 0$, $p_F \neq 0$ (pressure applied on the free surface). In both cases, we choose for the non-zero pressure

$$p(x, y) = \begin{cases} P_0 \exp\left(\dfrac{L^2}{x^2 - L^2} + \dfrac{L^2}{y^2 - L^2}\right), & |x| < L \text{ and } |y| < L, \\ 0 & \text{otherwise.} \end{cases} \tag{2.8}$$

Here, $P_0$ is a constant and $L$ defines the size of the support of the pressure. We introduce dimensionless variables by using $U$ as the unit velocity and $L$ as the unit length.

Combining (2.2) with (2.3), and (2.4) with (2.5), and using the chain rule we obtain

$$\frac{1}{2}\frac{\left(1+\zeta_x^2\right)\phi_{1y}^2 + \left(1+\zeta_y^2\right)\phi_{1x}^2 - 2\zeta_x\zeta_y\phi_{1x}\phi_{1y}}{1+\zeta_x^2+\zeta_y^2} - \frac{R}{2}\frac{\left(1+\zeta_x^2\right)\phi_{2y}^2 + \left(1+\zeta_y^2\right)\phi_{2x}^2 - 2\zeta_x\zeta_y\phi_{2x}\phi_{2y}}{1+\zeta_x^2+\zeta_y^2} + \frac{1-R}{F^2}\zeta + \varepsilon P = \frac{1-R}{2}, \tag{2.9}$$

$$\frac{1}{2}\frac{\left(1+\zeta_{s_x}^2\right)\phi_{s_y}^2 + \left(1+\zeta_{s_y}^2\right)\phi_{s_x}^2 - 2\zeta_{s_x}\zeta_{s_y}\phi_{s_x}\phi_{s_y}}{1+\zeta_{s_x}^2+\zeta_{s_y}^2} + \frac{\zeta_s}{F^2} = \frac{1}{2}, \tag{2.10}$$

where $\phi_i(x, y) = \Phi_i(x, y, \zeta(x, y))$ $(i = 1, 2)$, $\phi_s = \Phi_2(x, y, \zeta_s(x, y) + H)$, $F = U/(gL)^{1/2}$ is the Froude number, $R = \rho_2/\rho_1$ is the density ratio, $H = h/L$ is the relative thickness of the upper layer, $\varepsilon = P_0/\rho_1 U^2$ is the dimensionless magnitude of the pressure and $P = p/P_0$.

### 2.2. *Numerical method*

The numerical scheme is an extension to a two-fluid system of that used by Părău & Vanden-Broeck (2002) for the computation of forced gravity waves in deep water and by Părău *et al.* (2007) for forced interfacial gravity waves. It is based on a desingularized boundary integral-equation method introduced by Landweber & Macagno (1969) for the problem of uniform flow past an ellipsoid and generalized by Forbes (1989) for three-dimensional gravity free-surface flows past a source.

The formulation involves applying in each fluid Green's second identity to the functions $\Phi_i - x$ $(i = 1, 2)$ and $G$, where $G(P, P^*)$ is the three-dimensional free-space

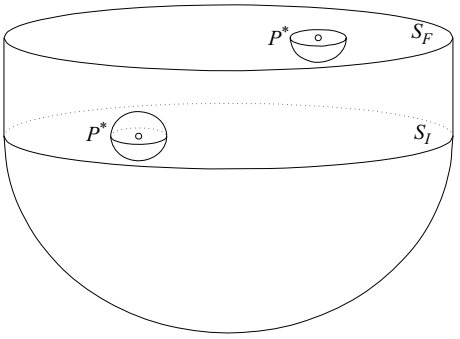


FIGURE 2. Sketch of the regions $V_1$ and $V_2$.

Green function

$$G(P, P^*) = \frac{1}{4\pi} \frac{1}{([x - x^*]^2 + [y - y^*]^2 + [z - z^*]^2)^{1/2}}, \tag{2.11}$$

in the regions $V_1$ and $V_2$. Here, $P = (x, y, z)$, $P^* = (x^*, y^*, z^*) \in S_I$. The region $V_1$ consists of a large-radius hemisphere bounded above by the interface $S_I$, except for a small hemisphere around the point $P^*$, and the region $V_2$ consists of a large-radius cylinder bounded by the free surface $S_F$ and the interface $S_I$, except for a small hemisphere around the point $P^*$ (see figure 2). Another integral equation is obtained when $P^*$ is on the free surface $S_F$ and Green's second identity is applied to the region $V_2'$, which is the same as $V_2$, except for a small hemisphere around the point $P^*$ on the free surface.

This yields the following equations

$$\tfrac{1}{2}(\Phi_1(P^*) - x^*) = \int_{S_I} (\Phi_1(P) - x) \frac{\partial G(P, P^*)}{\partial n_1} - G(P, P^*) \frac{\partial (\Phi_1(P) - x)}{\partial n_1} \mathrm{d}S_P \quad \text{for } P^* \in S_I,$$

$$\tfrac{1}{2}(\Phi_2(P^*) - x^*) = \int_{S_I} (\Phi_2(P) - x) \frac{\partial G(P, P^*)}{\partial n_2} - G(P, P^*) \frac{\partial (\Phi_2(P) - x)}{\partial n_2} \mathrm{d}S_P$$
$$+ \int_{S_F} (\Phi_2(P) - x) \frac{\partial G(P, P^*)}{\partial n_s} - G(P, P^*) \frac{\partial (\Phi_2(P) - x)}{\partial n_s} \mathrm{d}S_P$$

for $P^* \in S_I$, $P^* \in S_F$, where $n_i$ $(i = 1, 2)$ is the normal vector at the interface pointing into fluid $i$, and $n_s$ is the normal vector at the free surface.

The integro-differential equations are projected onto the $Oxy$-plane and the singularities in the integrands are isolated by addition and subtraction of a function whose integral can be evaluated in closed form (see Landweber & Macagno 1969; Forbes 1989; Părău & Vanden-Broeck 2002; Părău *et al.* 2007 for details). For the numerical scheme, we truncate the intervals $-\infty < x < \infty$ and $0 \leqslant y < \infty$ to $x_1 \leqslant x \leqslant x_N$, and $y_1 \leqslant y \leqslant y_M$ and introduce the mesh points $x_k = (k-1)\Delta x$, $k = 1, \ldots, N$ and $y_j = (j-1)\Delta y$, $j = 1, \ldots, M$. The $5NM$ unknowns are the values of $\zeta_x$, $\zeta_{s_x}$, $\phi_{1x}$, $\phi_{2x}$, $\phi_{s_x}$ at the mesh points. The integrals and the Bernoulli equation are evaluated at the points $(x_{k+1/2}, y_j)$, $k = 1, \ldots, N-1$, $j = 1, \ldots, M$ so we have $5(N-1)M$ equations. Another $5M$ equations are obtained from the radiation condition (see Părău & Vanden-Broeck 2002; Părău *et al.* 2007 for details). The values of $\zeta$ and $\zeta_s$ are obtained by integrating $\zeta_x$ and $\zeta_{s_x}$ with respect to $x$ by the trapezoidal rule. The values of the dependent variables at midpoints are found by interpolation and the derivatives are calculated by using finite differences. The $5NM$ nonlinear equations are solved by a modified

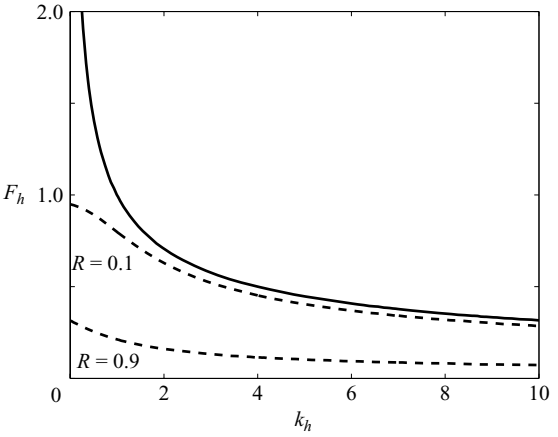


FIGURE 3. Dispersion curves $F_h^s$ (solid line) and $F_h^i$ (dashed lines) in the $(k_h, F_h)$-plane for $R = 0.1$ and $R = 0.9$.

Newton's method. In most computations, we used $N = 50$, $M = 20$, $\Delta x = \Delta y = 0.4$ or $N = 60$, $M = 20$, $\Delta x = \Delta y = 0.2$.

### 2.3. *Results*

Some insight can be gained by first reviewing the linear theory. Consider travelling waves with a wavenumber $\kappa = \sqrt{k^2 + l^2}$, where $k$ and $l$ are the wavenumber components along the propagation in the $x$-direction and $y$-direction, respectively (see Lamb 1932, Art. 231). The dispersion relation is then

$$F^4(1 + R\tanh\kappa H) - F^2\frac{\kappa}{k^2}(1 + \tanh\kappa H) + \frac{\kappa^2}{k^4}(1 - R)\tanh\kappa H = 0. \tag{2.12}$$

Considering only waves travelling along the $x$-direction ($l = 0$) and solving the equation (2.12) we obtain two positive roots for $F$, corresponding to two possible systems of waves:

$$F^s = \frac{1}{\sqrt{k}}, \quad F^i = \frac{1}{\sqrt{k}}\sqrt{\frac{(1 - R)\tanh kH}{1 + R\tanh kH}}.$$

The first solution $F^s$ corresponds to the so-called surface-wave mode, since it does not depend on $R$ and it can be obtained if we consider a single fluid of infinite depth. The second solution $F^i$ corresponds to the so-called internal-wave mode.

We will plot the two solutions. We do it in the $(k_h, F_h)$-plane instead of the $(k, F)$-plane, where $F_h = U/\sqrt{gh}$ is the Froude number based on the depth $h$ of the upper-layer thickness and $k_h$ the wavenumber non-dimensionalized with $h$. We should note that $F = F_h\sqrt{H}$. The two solutions are now

$$F_h^s = \frac{1}{\sqrt{k_h}}, \quad F_h^i = \frac{1}{\sqrt{k_h}}\sqrt{\frac{(1 - R)\tanh k_h}{1 + R\tanh k_h}}.$$

These are plotted in figure 3 for $R = 0.1$ and $R = 0.9$. We can observe that for a fixed $F_h < F_h^i(0) = \sqrt{1 - R}$, there are transverse waves (i.e. waves travelling in the $x$-direction with crests perpendicular to the direction of propagation). These are generated by the surface-wave mode (solid line) and the interface-wave mode (dashed line). For a fixed $F_h > \sqrt{1 - R}$ there are transverse waves generated only by the surface-wave mode.

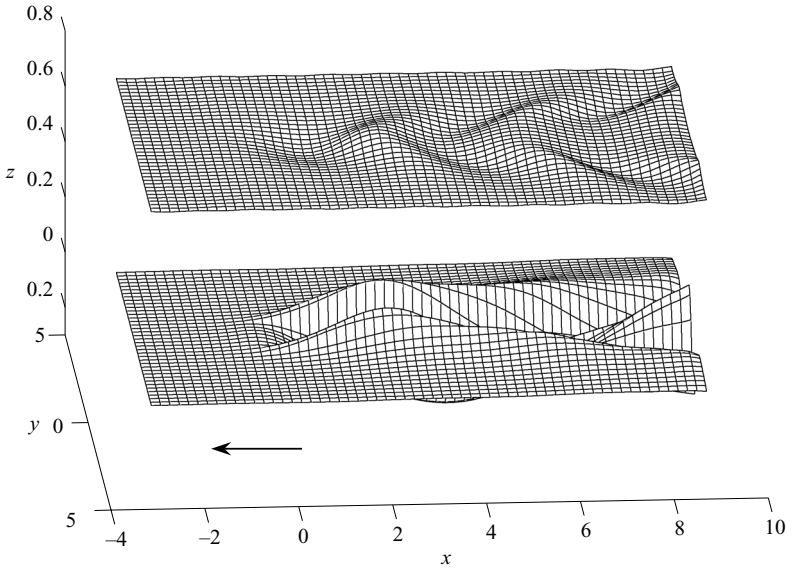


FIGURE 4. Computed free-surface and interface profiles. The pressure is applied on the interface and the parameters are $F = 0.7$, $R = 0.9$, $H = 0.7$, $\varepsilon = 1$.

Other possible waves are the divergent waves (i.e. having crests diverging from the pressure support) due to the surface-wave mode and internal-wave mode. The transverse and divergent waves for each mode are similar to those in the classical Kelvin wake pattern, which were first described by Lord Kelvin (Thompson 1887). So each wave-pattern on the interface and on the free surface can be composed of up to four different wave systems: divergent waves and transverse waves due to the surface wave mode, and the divergent and transverse waves due to the internal wave mode.

The numerical scheme was used to calculate solutions for different values of the Froude number $F$, density ratio $R$, the relative thickness of the upper layer $H$, and the pressure parameter $\varepsilon$.

First, we will present results with the pressure applied on the interface. A typical result for the supercritical case, when $F > F^i(0) = \sqrt{(1-R)H}$ is shown in figure 4. The Kelvin wake, with transverse and divergent waves, is visible on the free surface, whereas on the interface there are only divergent waves. The waves on the free surface are due to the surface-wave mode, as the internal-wave mode has negligible effect on it, whereas the waves on the interface are generated by the internal-wave mode.

The accuracy of the solutions has been tested by varying the number of grid points and the distances $\Delta x$ and $\Delta y$ between grid points (see an example in figure 5). The upper part of the interface and the free surface, $y > 0$ is calculated with $N = 60$, $M = 30$, $\Delta x = \Delta y = 0.4$ and the lower part $y < 0$ is calculated with $N = 60$, $M = 30$, $\Delta x = \Delta y = 0.3$. The values of the parameters are the same in both cases ($F = 0.7$, $R = 0.9$, $H = 1$ and $\varepsilon = 1$).

The subcritical case, when there are transverse and divergent waves on both free surface and interface is presented in figure 6. As in the previous example, the surface-wave mode affects mainly the free-surface waves, whereas the internal-wave mode effects mainly the interfacial waves. It can also be observed that the waves generated by the internal-wave mode are longer than the waves due to the surface-wave mode.

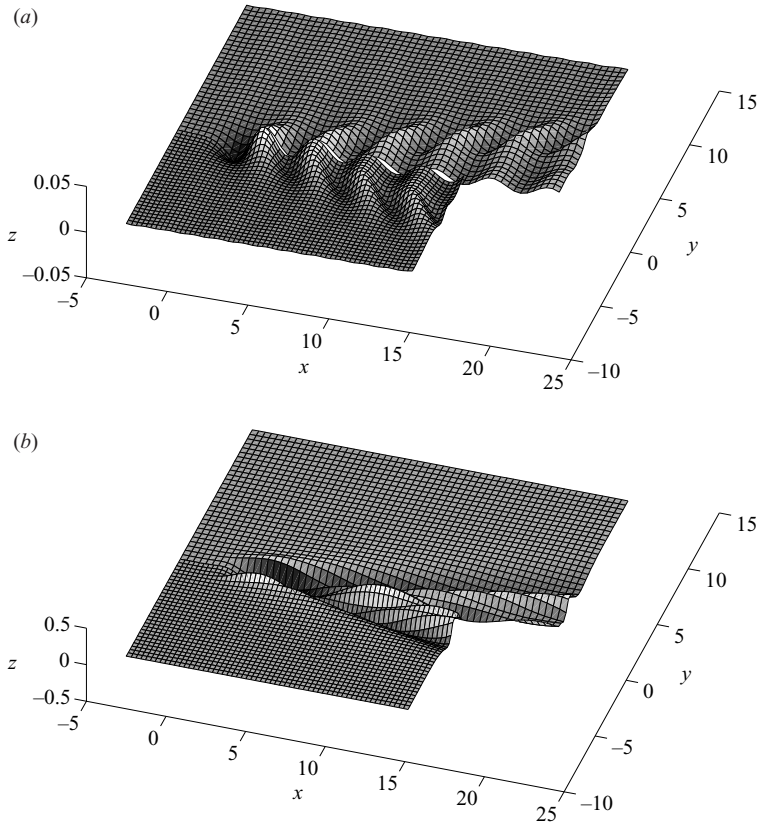


FIGURE 5. Profiles of (*a*) the free surface and of (*b*) the interface for two different grids: $\Delta x = \Delta y = 0.3$ for $y < 0$ and $\Delta x = \Delta y = 0.4$ for $y > 0$. The parameters are $F = 0.7$, $R = 0.9$, $H = 1$.

For some values of parameters, for example, when the relative height $H$ of the upper layer is small, or when the density ratio $R$ is not so close to 1, we observed the influence of the surface-wave mode and internal-wave mode on both the free surface and the interface. In figure 7, this can be observed clearly on the free surface, where, besides the classical Kelvin wake, there are some divergent waves due to the internal wave-mode which are not confined to the 38° angle. They are out of phase with the waves on the interface, as the crests on the free surface are exactly over the troughs on the interface.

For the supercritical case, we were able to compute solutions with the so-called triple-lobe pattern on the interface, predicted by Tulin & Miloh (1991) and Tulin, Wang & Yao (1994) using perturbation crossflow theory and approximating the free surface as a rigid lid. The triple-lobe pattern consists of a sharp peak and two shallow troughs behind the moving pressure (figure 8). The free surface was present in our computations.

The influence of the surface-wave mode on the interfacial waves can be observed when the free surface is replaced by a rigid lid. The numerical scheme is similar to that derived in Părău *et al.* (2007), where solitary waves between two semi-infinite fluids were computed, one difference being the choice of the region of integration considered for the upper fluid. In this case we replaced the large-radius hemisphere

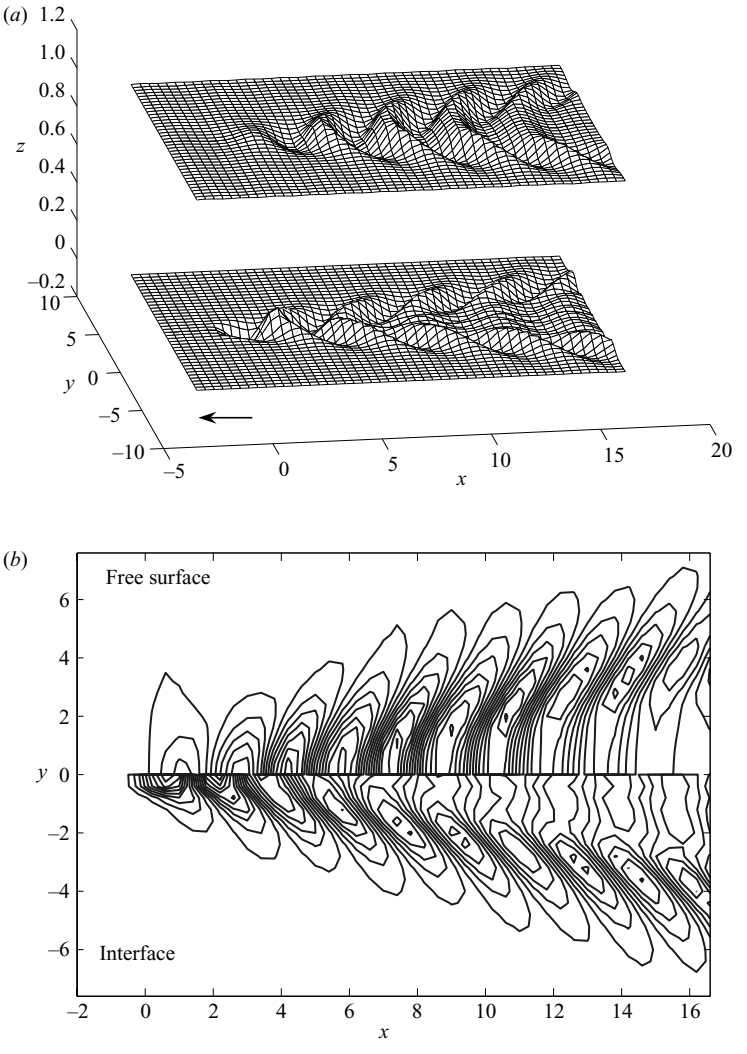


FIGURE 6. (*a*) Free surface and interface and (*b*) a contour plot. The parameters are $F = 0.6$, $R = 0.1$, $H = 1$.

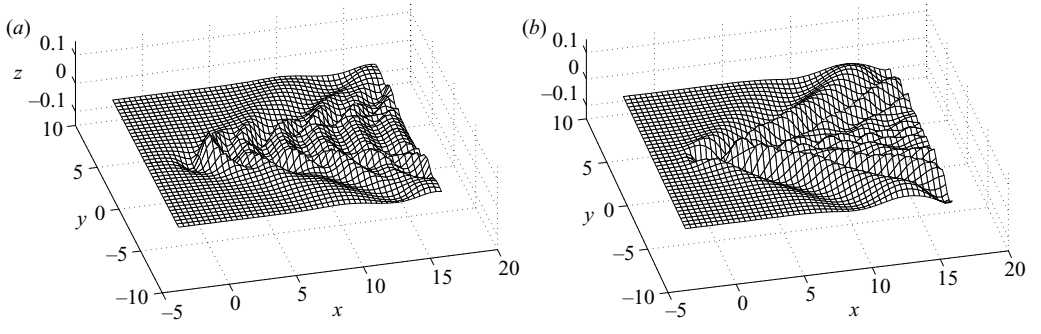


FIGURE 7. (*a*) Free surface and (*b*) interface. The parameters are $F = 0.6$, $R = 0.5$, $H = 0.5$.

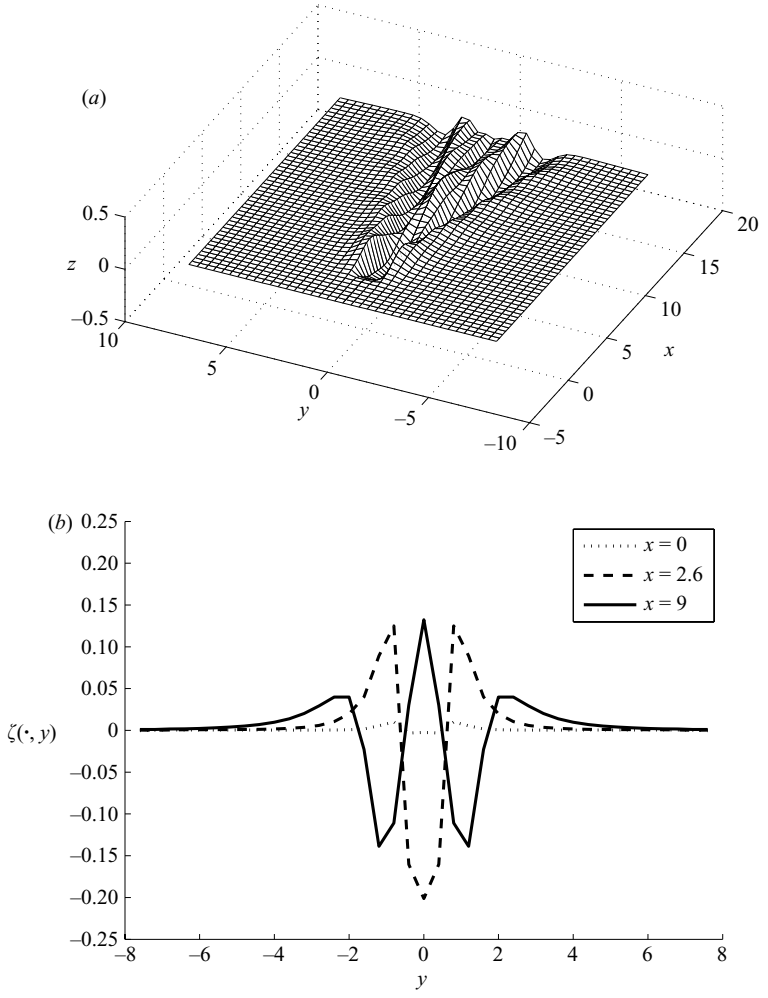


FIGURE 8. (*a*) The interface. (*b*) Transverse sections of the interface. The parameters are $F = 0.7$, $R = 0.9$, $H = 0.5$.

with a large-radius cylinder, the upper face being the reflection of the interface in the rigid lid. In figure 9 we compared the interfacial waves for the two cases. The centrelines in the $x$-direction are presented for the solution with a rigid lid $\zeta_{lid}$ and for the solution with a free surface $\zeta$. If we compare the centreline of the free surface $\zeta_s$ with the difference between those two, it can be observed that the small waves on the interface $\zeta$ are generated by the free-surface mode.

We can apply the pressure on the free surface instead of the interface. In the cases presented here, in figure 10, the surface-wave mode dominated on both the free surface and the interface. As we increase the height $H$ of the upper layer, the amplitude of the interfacial waves decreases; the free-surface waves remain almost unchanged.

For $R = 0.5$, we can find solutions where the coupling effect of the surface-wave mode and internal-wave mode is visible on both surfaces (see figure 11).

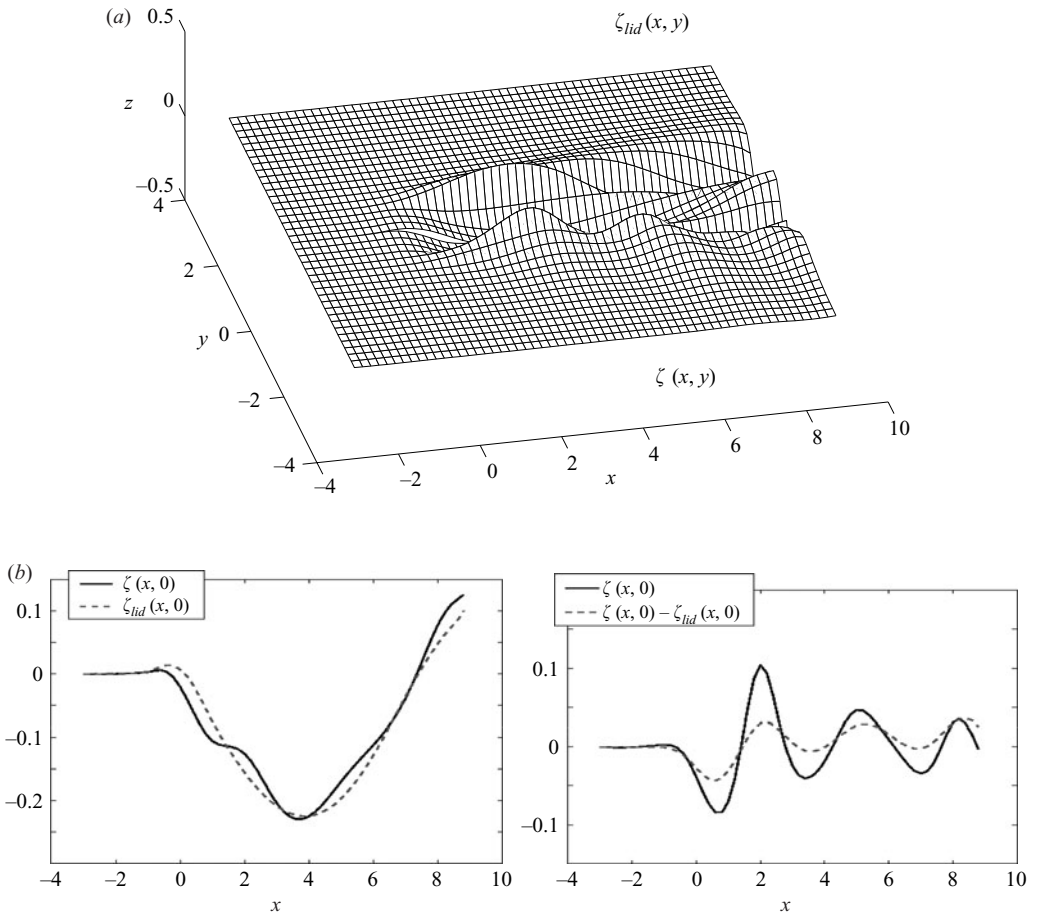


FIGURE 9. (*a*) Interface profile with a free surface for $y < 0$ and with a rigid lid on top for $y > 0$. (*b*) Centrelines at $y = 0$ in $x$-direction. The parameters are $F = 0.7$, $R = 0.9$, $H = 0.3$.

## 3. Gravity–capillary interfacial solitary waves

We are interested in finding fully localized gravity–capillary interfacial solitary waves when the upper fluid is covered by a rigid lid. The dynamical condition (2.3) at the interface $z = \zeta(x, y)$ becomes

$$\tfrac{1}{2}\rho_1\left(\Phi_{1x}^2 + \Phi_{1y}^2 + \Phi_{1z}^2\right) - \tfrac{1}{2}\rho_2\left(\Phi_{2x}^2 + \Phi_{2y}^2 + \Phi_{2z}^2\right) + (\rho_1 - \rho_2)g\zeta - T\left[\frac{\zeta_x}{\sqrt{1 + \zeta_x^2 + \zeta_y^2}}\right]_x - T\left[\frac{\zeta_y}{\sqrt{1 + \zeta_x^2 + \zeta_y^2}}\right]_y = \tfrac{1}{2}(\rho_1 - \rho_2)U^2, \quad (3.1)$$

where $U$ is now the phase speed of the wave.

Kim & Akylas (2006, equation (3.1)) have derived a weakly nonlinear model equation for gravity–capillary interfacial waves in this case (two-dimensional Benjamin equation), when the interfacial tension $T$ is large and $\rho_1 \approx \rho_2$:

$$(-\zeta_x + (\zeta^2)_x - 2\gamma\mathscr{H}\{\zeta_{xx}\} + \zeta_{xxx})_x - \zeta_{yy} = 0,$$

where $\gamma^2 = 1 - R/4R^2\beta F^2$, $\beta = T/\rho_1 h U^2$, $F^2 = U^2/gh$ and $\mathscr{H}$ is the Hilbert transform.

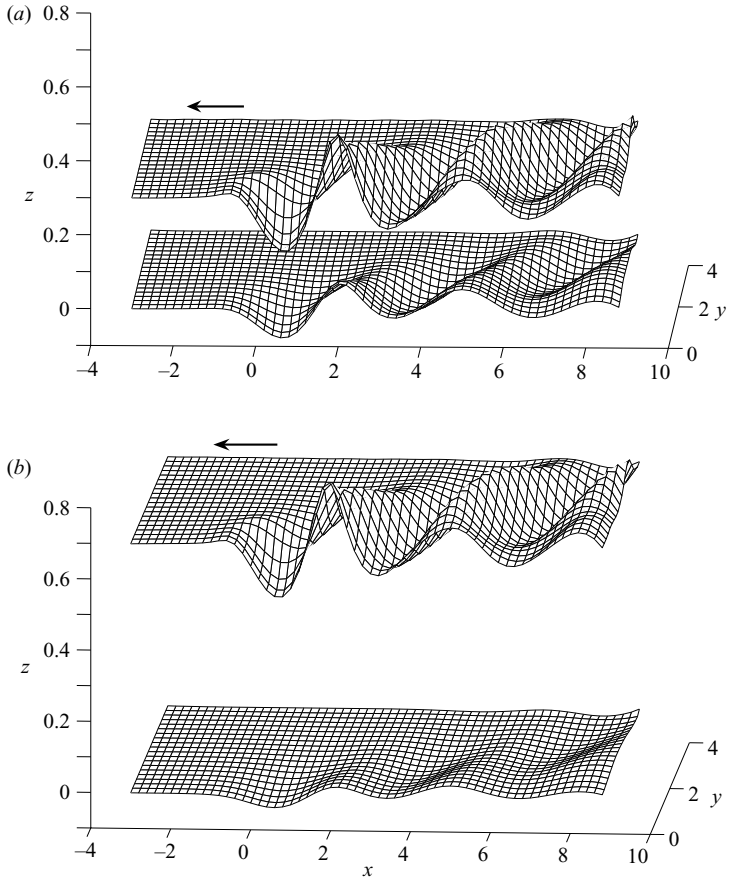


FIGURE 10. Solutions when the pressure distribution is at the free surface. The parameters are (*a*) $F = 0.7$, $R = 0.9$, $H = 0.3$ and (*b*) $F = 0.7$, $R = 0.9$, $H = 0.7$.

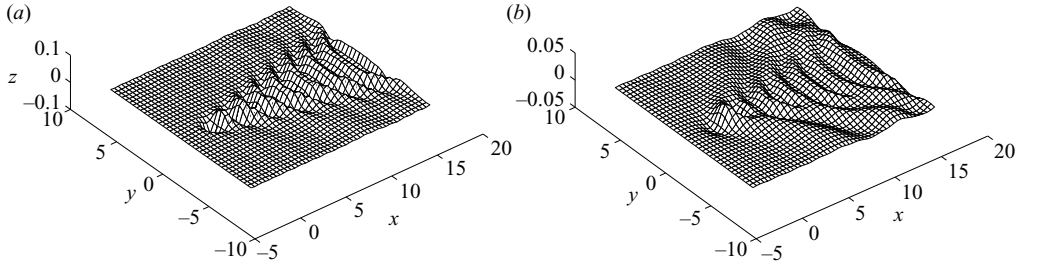


FIGURE 11. (*a*) The free surface and (*b*) the interface, when the pressure distribution is at the free surface. The parameters are $F = 0.5$, $R = 0.5$, $H = 0.5$.

The phase-speed of the waves satisfying this equation has a minimum. In the neighbourhood of this minimum, Kim & Akylas (2006) have used an asymptotic method to show that the envelope of these waves satisfies an elliptic–elliptic Davey–Stewartson (or Benney–Roskes) system. By solving these equations numerically, they were able to find three-dimensional fully localized solitary-wave solutions. We should mention that a similar Davey–Stewartson system was derived by a weakly nonlinear method by Kim & Akylas (2005) for free-surface gravity–capillary waves in finite depth, which also admits fully localized solitary-wave solutions.

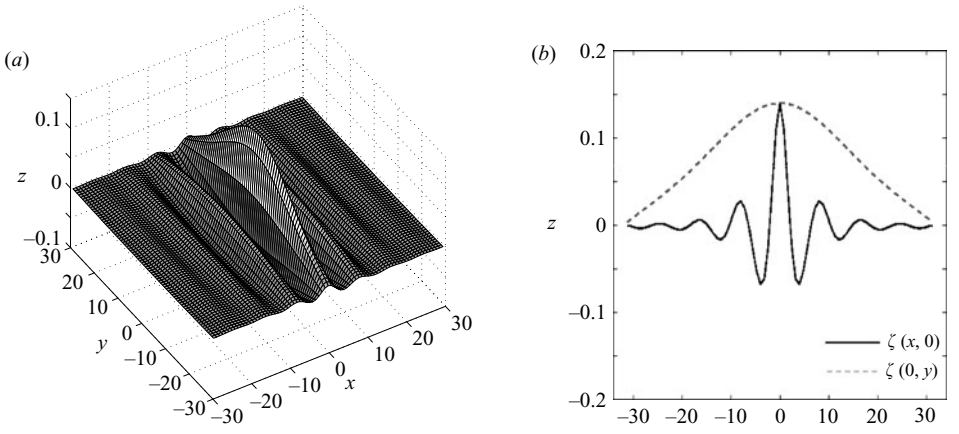


FIGURE 12. (*a*) An elevation gravity–capillary interfacial solitary wave. (*b*) Centreline sections in the $x$- and $y$-directions. The parameters are $F = 0.76$, $\beta = 1$, $R = 0.5$.

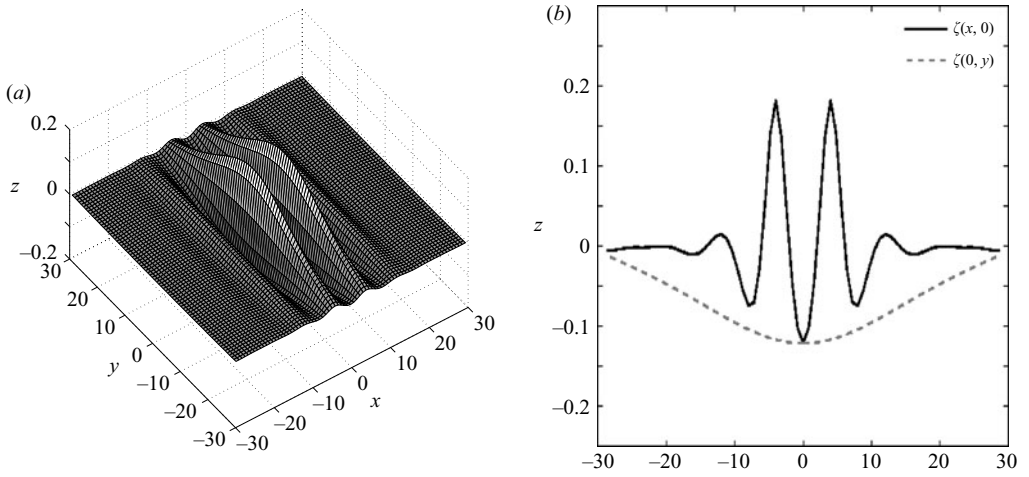


FIGURE 13. (*a*) A depression gravity–capillary interfacial solitary wave. (*b*) Centreline sections in the $x$- and $y$-directions. The parameters are $F = 0.75$, $\beta = 1$, $R = 0.5$.

We consider now the linear dispersion relation, for travelling waves in the $x$-direction, for the full interfacial equations (see Benjamin 1992):

$$\frac{1 - R + \beta F^2 k^2}{|k| + Rk \coth k} - F^2 = 0.$$

If $k = k_0$ is a double root of this equation, it corresponds to a phase-speed minimum (see Calvo & Akylas 2003). We have computed three-dimensional fully localized solitary waves for $k$ near $k_0$ for the full nonlinear equations, to confirm the weakly nonlinear results. The numerical procedure used is similar to that described in § 2, the higher-order derivatives that appear are treated as in the free-surface case (see Părău *et al.* 2005*a*). The numerical results shown below were obtained with $N = M = 40$, $\Delta x = \Delta y = 0.8$.

There are two families of fully localized solitary waves which bifurcate from a two-dimensional periodic wave. We present an example from each family: one family has a central elevation (see figure 12), the other has a central depression (see figure 13)

at $x = y = 0$. Similar to the free-surface problem discussed in Părău *et al.* (2005*a*), the waves have decaying oscillations in the direction of propagation and monotonic decay perpendicular to the direction of propagation. We also observed that, unlike the free-surface waves, the interfacial waves have shallow troughs and tall crests. A similar observation was made for the two-dimensional case in Calvo & Akylas (2003). The branch of solutions can be followed numerically far from the minimum phase-speed, which, for fixed $\beta = 1$ and $R = 0.5$, is found at $F_c = 0.79$.

## 4. Conclusions

We have presented two different types of solution for interfacial flows. First we have calculated three-dimensional gravity waves generated by moving pressures in two-layer fluid configurations, with a free surface. The full nonlinear problem was solved numerically and previous linear and weakly nonlinear results were confirmed and extended. Secondly, we have computed fully localized gravity–capillary interfacial solitary waves near the minimum phase-speed, when the free surface is replaced by a rigid lid. The solutions found confirm the results of Kim & Akylas (2006) who used a weakly nonlinear model.

This work was supported by EPSRC, under Grant GR/S47786/01 and the National Science Foundation.

## REFERENCES

Avital, E. & Miloh, T. 1998 On an inverse problem of ship-induced internal waves. *Ocean Engng* **26**, 99–110.

Benjamin, T. B. 1992 A new kind of solitary wave. *J. Fluid Mech.* **245**, 401–411.

Calvo, D. C. & Akylas, T. R. 2003 On interfacial gravity–capillary solitary waves of the Benjamin type and their stability. *Phys. Fluids* **15**, 1261–1270.

Crapper, G. D. 1967 Ship waves in a stratified ocean. *J. Fluid Mech.* **29**, 667–672.

Dias, F. & Iooss, G. 1996 Capillary–gravity interfacial waves in infinite depth. *Eur. J. Mech.* B/*Fluids* **15**, 367–393.

Ekman, V. W. 1904 On dead water. *Norwegian North Polar Expedition, 1893–1896, Scientific Results* vol. 5, pp. 1–150.

Forbes, L. K. 1989 An algorithm for 3-dimensional free-surface problems in hydrodynamics. *J. Comput. Phys.* **82**, 330–347.

Hudimac, A. A. 1961 Ship waves in a stratified ocean. *J. Fluid Mech.* **10**, 229–243.

Hughes, B. A. 1986 Surface wave wakes and internal waves wakes produced by surface ships. *Proc. 16th Symp. Naval Hydrodyn. Berkeley, CA*, pp. 1–17.

Keller, J. B. & Munk, W. H. 1970 Internal wave wakes of a body moving in a stratified fluid. *Phys. Fluids* **13**, 1425–1431.

Kim, B. & Akylas, T. R. 2005 On gravity–capillary lumps. *J. Fluid Mech.* **540**, 337–351.

Kim, B. & Akylas, T. R. 2006 On gravity–capillary lumps. Part 2. Two-dimensional Benjamin equation. *J. Fluid Mech.* **557**, 237–256.

Laget, O. & Dias, F. 1997 Numerical computation of capillary–gravity interfacial solitary waves. *J. Fluid Mech.* **349**, 221–251.

Lamb, H. 1932 *Hydrodynamics*, 6th edn. Cambridge University Press.

Landweber, L. & Macagno, M. 1969 Irrotational flow about ship forms. *Iowa Institute of Hydraulic Research Rep.* IIHR 123, 1–33.

Părău, E. I. & Vanden-Broeck, J.-M. 2002 Nonlinear two and three dimensional free surface flows due to moving disturbances. *Eur. J. Mech.* B/*Fluids* **21**, 643–656.

Părău, E. I., Vanden-Broeck, J.-M. & Cooker, M. J. 2005*a* Nonlinear three-dimensional gravity–capillary solitary waves. *J. Fluid Mech.* **536**, 99–105.

Părău, E. I., Vanden-Broeck, J.-M. & Cooker, M. J. 2005*b* Three-dimensional gravity–capillary solitary waves in water of finite depth and related problems. *Phys. Fluids* **17** (12), 122101.

Părău, E. I., Vanden-Broeck, J.-M. & Cooker, M. J. 2007 Three-dimensional gravity and gravity–capillary interfacial flows. *Math. Comput. Simulation* **74**, 105–112.

Thompson, W. 1887 On ship waves. *Proc. I Mech. E* Reprint 1891. In *Popular Lectures and Addresses* vol. 3, pp. 450–500.

Tulin. M. P. & Miloh, T. 1991 Ship internal waves in a shallow thermocline: the supersonic case. *Proc. 18th Symp. Naval Hydrodyn.*, pp. 567–581, National Academy Press.

Tulin, M. P., Wang, P. & Yao, Y. 1994 Numerical prediction of ship generated internal waves in a stratified ocean at supercritical Froude numbers. *Proc. 6th Intl Conf. Numerical Ship Hydrodyn.* pp. 289–309, National Academy Press.

Wey, G., Lu D. & Dai, S. 2005 Waves induced by a submerged moving dipole in a two-layer fluid of finite depth. *Acta Mec. Sin.* **21**, 24–31.

Yeung, R. W. & Nguyen, T. C. 1999 Waves generated by a moving source in a two-layer ocean of finite depth. *J. Engng Maths* **35**, 85–107.

Yih, C. S & Zhu, S. 1989 Patterns of ship waves. *Q. Appl. Maths* **47**, 17–33.